

We are IntechOpen, the world's leading publisher of Open Access books Built by scientists, for scientists

6,900

Open access books available

186,000

International authors and editors

200M

Downloads

Our authors are among the

154

Countries delivered to

TOP 1%

most cited scientists

12.2%

Contributors from top 500 universities



WEB OF SCIENCE™

Selection of our books indexed in the Book Citation Index
in Web of Science™ Core Collection (BKCI)

Interested in publishing with us?
Contact book.department@intechopen.com

Numbers displayed above are based on latest data collected.
For more information visit www.intechopen.com



Thin-Film Diamond Phototransistors

Linjun Wang, Jian Huang, Ke Tang, Jijun Zhang and Yiben Xia
School of Materials Science and Engineering, Shanghai University, Shanghai 200072, China

1. Introduction

In 21st century, with optoelectronic integration technology fast developing, the new technology has put forward higher demand for devices operating in high-power, high-frequency, and high-temperature environment. Under the circumstances, the devices based on common used semiconductor materials (silicon, GaAs, etc.) more and more show the limitation of properties. The researches of new generation semiconductors suitable for application in severe environments (high-power, high-temperature, high radiation flux, etc.) focus on wide bandgap semiconductors such as SiC[1-2], GaN[3-4] and diamond.

The comparison of main properties between diamond, GaN, SiC and commonly used semiconductors are shown in table 1 [5-8], from which we can see that diamond is one the most promising candidate for new generation semiconductor material due to its unique properties, including wide bandgap, high carrier mobility, high hole-saturation velocity, highest thermal conductivity, high electric breakdown field, and chemical inertness, etc. In the past decades, the development of diamond-based devices are hampered by several problems, a big issue is the high price and rare resource of single diamond. However, in 1980s, the success of diamond film synthesis by chemical vapor deposition (CVD) have opened up the possibilities for a wide range of applications, such as high-temperature, high-power microelectronics device, and ultraviolet light emitting optoelectronics. Over the past few years a variety of state-of-the-art diamond film devices have been fabricated, analysed and simulated including field effect transistors (FET).

Two concepts have been developed concerning p-channel diamond film FETs: boron-doped surface channel FET and hydrogen-induced surface channel FET. However, boron is not an ideal dopant as at moderate concentration levels it displays a deep acceptor level of about 0.37eV resulting in low carrier densities at room temperature [9-10]. In 1989, Ravi and Landstrass[11] reported a substantial surface conductivity of hydrogenated diamond surfaces (p-type semiconducting layer), both of single crystals and of films prepared by chemical vapor deposition, respectively. This surface conductivity is unique among semiconductors and can be a promising candidate for the application in electronic devices due to the smaller acceptor activation energy less than 50meV [12-13].

While boron-doped channel FETs still encounter serious technological problems, hydrogen-terminated surface channels have been successfully used for the fabrication of Schottky diodes[14], metal semiconductor gate FETs (MESFETs) and metal-insulator gate FETs (MISFETs) [15]. To date, although some valuable information about this hydrogen-terminated surface conductivity of diamond has been obtained, it is still far from sufficient and more detailed research is indispensable.

Properties	diamond	β -SiC	GaAs	CdZnTe	GaN	Si
Atomic number /Z	6	14/6	31/33	48/30/52	31/7	14
Hardness/(GPa)	100	3.43	0.59			0.98
Bandgap/(ev)	5.5	3.0	1.43	1.5-2.2	3.45	1.12
Thermal expansion coefficient / (10 ⁻⁶ /°C)	1.1	4.7	5.9		5.6	2.6
Dielectric constant	5.7	9.7	12.5	10.9	9	11.8
Resistivity/($\Omega \cdot \text{cm}$)	>10 ¹³	150	108	10 ¹¹	>10 ¹⁰	105
Electron mobility / (cm ² /V s)	2200	400	8500	1350	1250	1500
Hole mobility / (cm ² / V s)	1800	50	400	120	850	600
Breakdown field/(10 ⁴ V/cm)	1000	400	40	0.15	>100	30
Thermal conductivity / (W cm ⁻¹ K ⁻¹)	20	5	0.46		1.3	1.5
Electron saturated velocity/(10 ⁷ cm/s)	2.7	2.5	1		2.2	1
Working temperature / (°C)	<800		130	300	>300	77

Table 1. Comparison of properties between diamond, GaN, SiC and commonly used semiconductors

In this paper, high quality freestanding diamond (FSD) films and formation of H-terminated p-type channel on the diamond film surface were investigated and the origin of this H-terminated high-conductivity layer was discussed. The realization and properties of the optically activated MESFETs were also described here.

2. Preparation and characterization of FSD films

In this work, a microwave plasma chemical vapour deposition (MPCVD) technique at 2.45 GHz using a gaseous mixture of methane, hydrogen was applied to deposit FSD films on p-type low resistivity single crystalline silicon substrates. All three gases were metered into the chamber using mass flow controllers. The deposition parameters for FSD films were shown in table 2.

Flux of hydrogen (sccm)	Flux of methane (sccm)	Chamber pressure (KPa)	Substrate temperature (°C)
100	1	4.5	800

Table 2. Parameters for FSD deposition

After deposition, the silicon substrates were chemically etched to obtain FSD films with a smooth surface at the nucleation side. The FSD films were disposed in mixed solution of H₂O₂ and H₂SO₄ for 15 min to eliminate non-diamond surface layer of the diamond films.

These samples were then cleaned by ultrasonic vibration in deionized water. A thermal annealing treatment in nitrogen atmosphere at 650°C for an hour was performed to further improve the quality of the diamond films. The thickness of the film was about 110µm, as shown in Fig.1.

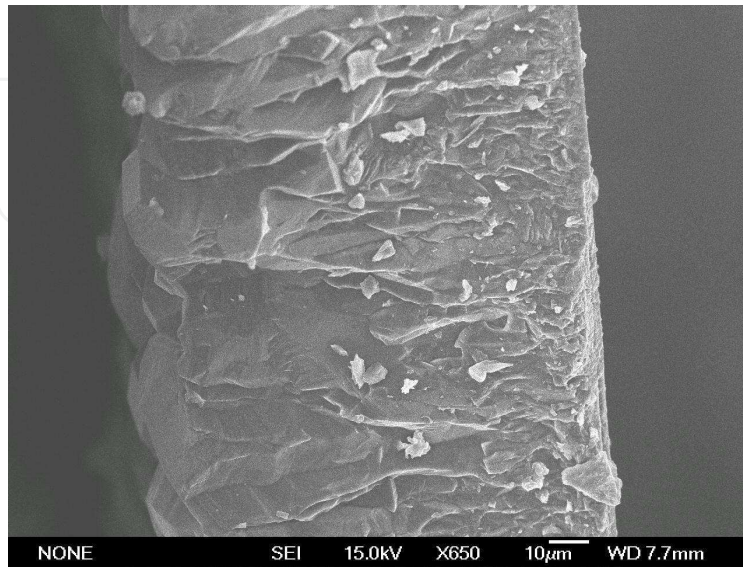


Fig. 1. Cross section image of the FSD film

Figure 2 and figure 3 showed SEM images of growth surface and nucleation surface of FSD films. The mean grain size of growth surface of the FSD film range from a few micrometers to tens of micrometers and the growth surface was very rough. Whereas, the nucleation surface was very smooth

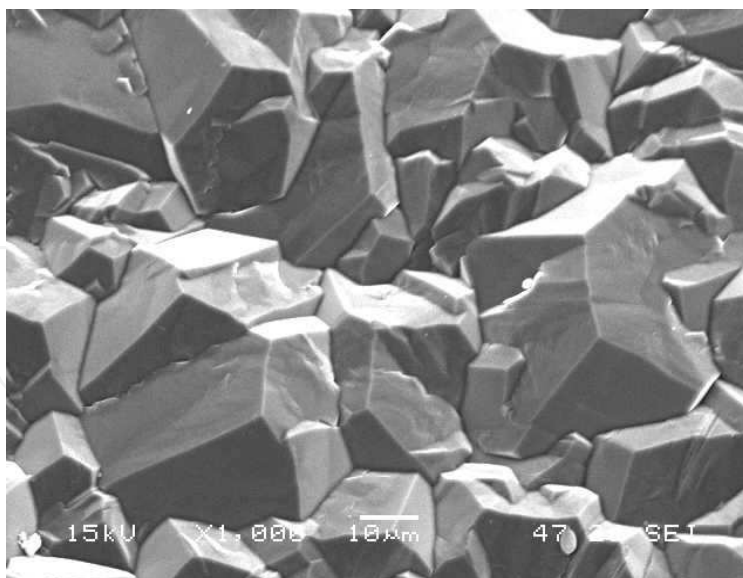


Fig. 2. SEM image of growth surface of FSD

The typical AFM images of the nucleation side of FSD film are shown in Fig. 4, from which it could be seen that the nucleation side was very smooth with a mean surface roughness of about 10 nm in a scanning area of 1.5×1.5 µm². The result was consistent with that obtained from SEM images.

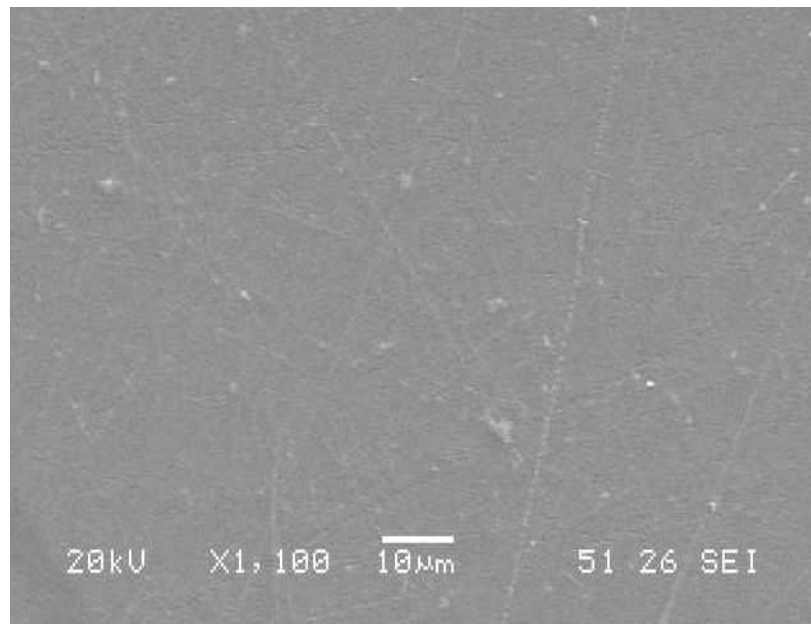


Fig. 3. SEM image of nucleation surface of FSD

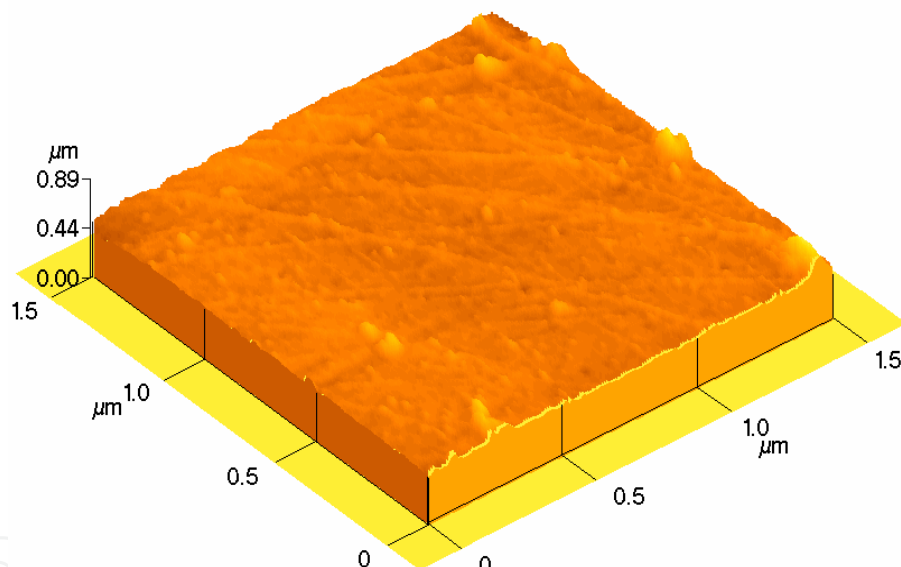


Fig. 4. AFM image of nucleation surface of FSD film

The Raman spectrum of the nucleation side of freestanding diamond film was shown in Fig.5. For both FSD films with and without post-treatment, a strong Raman scattering peak, located at about 1332cm^{-1} , is the characteristic of diamond and a weaker Raman scattering band, existed in range of $1400\sim 1600\text{cm}^{-1}$, is the characteristic of non-diamond carbon [16]. It is well known that the Raman signal for non-diamond carbon phase is about 75 times of that for diamond. So Raman spectroscopy is also used to estimate the non-diamond carbon content (C_{nd}) [17]: $C_{nd} = 1 / [1 + 75(I_{dia}/I_{nd})]$, where I_{dia} is Raman peak intensity for diamond crystals and I_{nd} is Raman peak intensity for non-diamond carbon phase. Therefore, the Raman results from Fig.5 indicated a high quality diamond of nucleation side of FSD diamond films with low content of non-diamond carbon. The Fig.5 also revealed that post-treatment (wet chemical etch, annealing process) was helpful to improve the quality of FSD films.

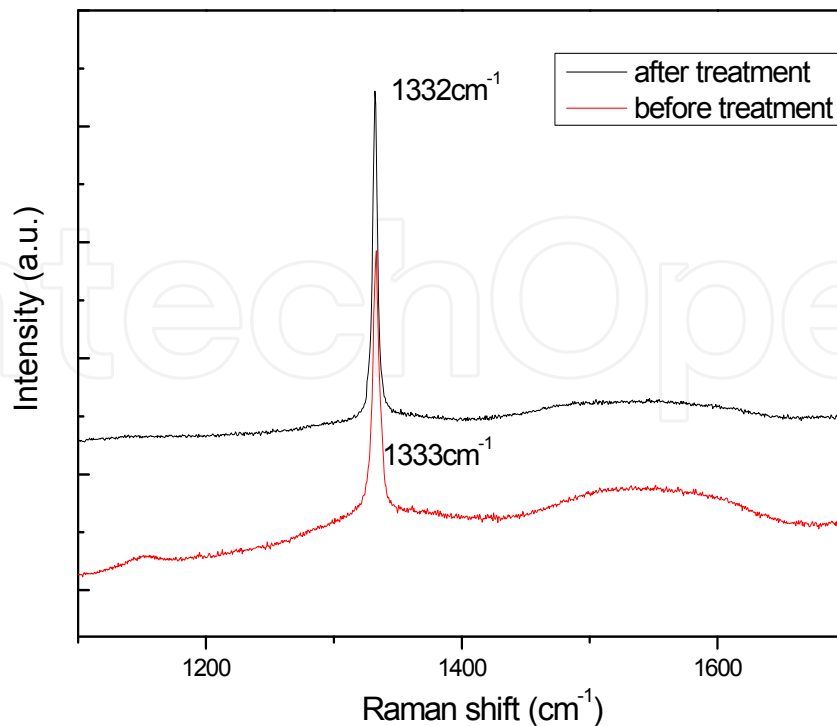


Fig. 5. Raman spectrum of nucleation side of freestanding diamond film

3. Preparation and characterization of H-terminated p-type channel on FSD films

The FSD films prepared above were exposed to hydrogen plasma at 750°C using a MPCVD apparatus. The time of hydrogen plasma treatment on the p-type behavior of undoped FSD nucleation surfaces were investigated by Hall Effect measurement. The electrical properties of the FSD nucleation surfaces following different annealing temperature were also measured.

Figure 6 shows the sheet carrier density and sheet resistivity of p-type FSD films as a function of time of hydrogen plasma treatment. The sheet carrier density rises with the time of hydrogen plasma treatment and a stable value is achieved after about 30 min, whereas the sheet resistivity reduces with time, with stable value being achieved after the same period of time.

The sheet carrier density and sheet resistivity of p-type FSD films as a function of annealing temperature in air and in vacuum were shown in Fig.7 and Fig.8, respectively. All the FSD films are exposed to hydrogen plasma treatment for 30 min at 750°C before a 180 min annealing process. The values of sheet carrier density and sheet resistivity remained in a relative stable range but change dramatically after annealing at temperature above 250 °C in air, whereas the sheet carrier density and sheet resistivity kept a stable value up to 600°C in vacuum.

Figure 9 and Fig.10 showed the values of sheet carrier density and sheet resistivity obtained as a function of time that a sample had been annealed at various temperatures in air. The data presented are typical of that obtained for many samples. Following annealing at 100 °C, little variation was apparent in measurements taken over a prolonged period. However, if the film was annealed at higher temperatures of 200 °C and 250°C the sheet carrier density was seen to decrease with time, although a stable value was reached after a given period,

whereas the film resistivity showed a reversed trend, gradually increasing to a stable resistivity with the increase of annealing.

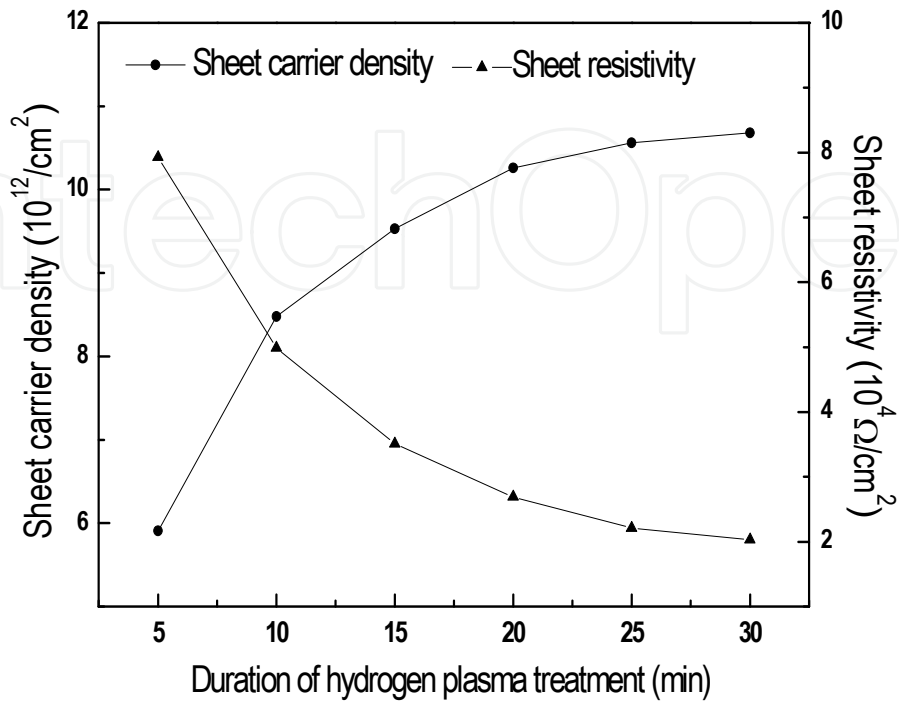


Fig. 6. Sheet carrier density and sheet resistivity of FSD against duration of hydrogen plasma treatment

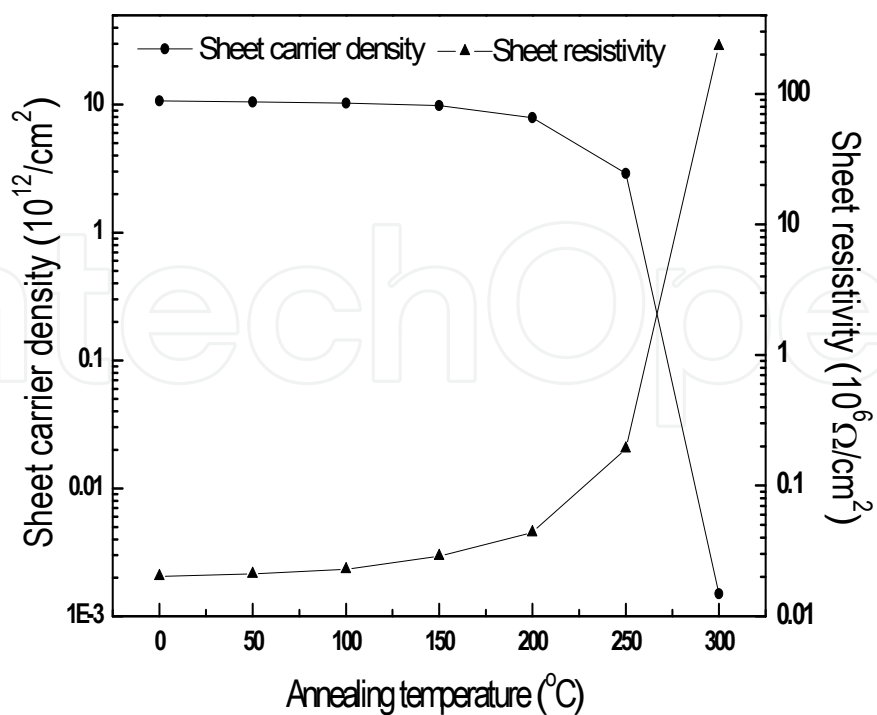


Fig. 7. Sheet carrier density and sheet resistivity of FSD against annealing temperature in air

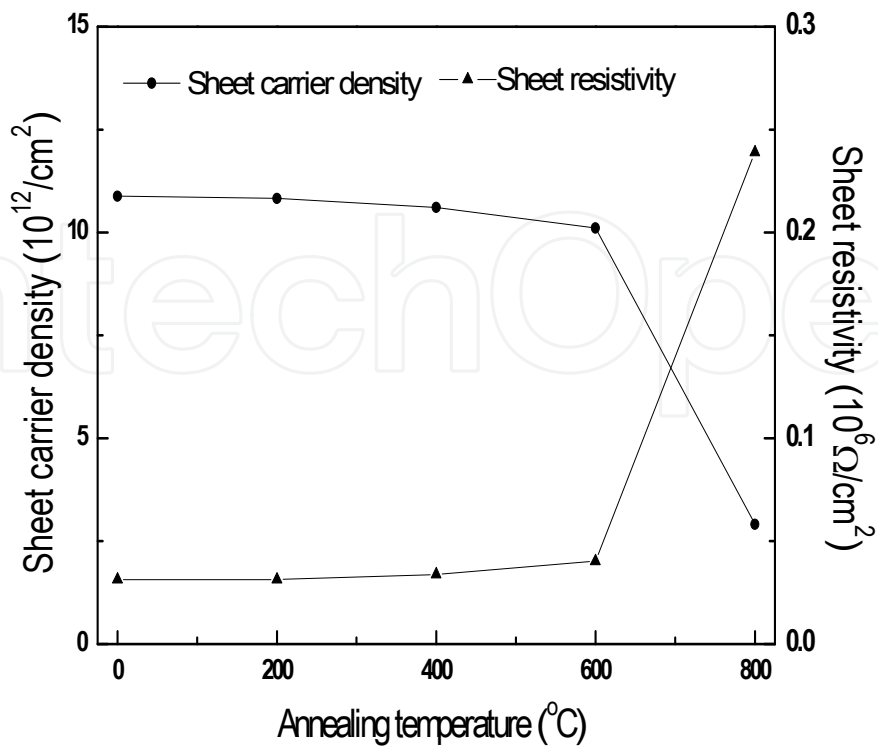


Fig. 8. Sheet carrier density and sheet resistivity of FSD against annealing temperature in vacuum

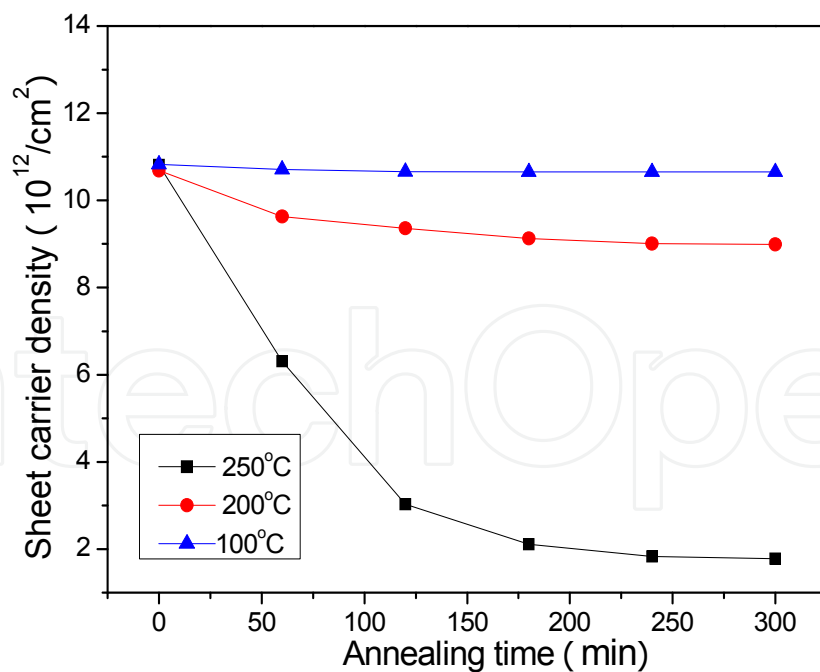


Fig. 9. Sheet carrier density against time of annealing

It's well known that the growth of diamond films at low pressure is a kinetic nonequilibrium process because of the thermodynamic instability of diamond under these conditions [18]. During such a nonequilibrium growth process, hydrogen plasma or atomic

hydrogen radicals get rid of the graphitic phase, and sp^3 species are rearranged to form crystalline diamond by gradually adjusting their positions and orientations near the growth face region [19]. The incompletely grown subsurface layer, where vacancies and dangling bonds were concentrated, was continuously transformed into the “perfect” bulk diamond [20]. Thus an imperfect thin layer will always exist on the diamond growth face. Hayashi et al. also reported that high density hydrogen was incorporated into the subsurface region rather than in bulk of as-grown diamond films by secondary ion mass spectroscopy (SIMS) [21]. Therefore, the diamond surface conductivity may be related to the complexes of absorbed hydrogen atoms with carbon dangling bonds. For example, if two adjacent carbon-dangling bonds share one hydrogen atom, an acceptor state should be generated in the band gap, since each hydrogen atom has only one electron.

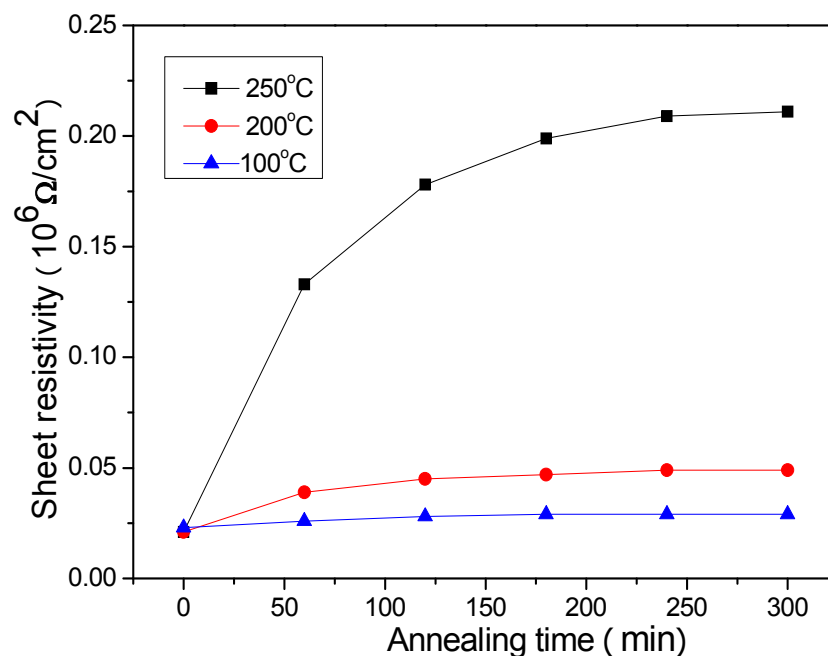


Fig. 10. Sheet resistivity against time of annealing

Starting from this point, the above experimental results can be well understood. The nucleation surface of the CVD diamond film is full of defects (e.g., vacancies, dangling bonds). The hydrogen plasma treatment may promote the complexes of hydrogen atoms with vacancies and dangling bonds. After a period of time, a stable value of the sheet carrier density is achieved when almost all the vacancies and dangling bonds are hydrogenated. The sheet carrier density reduces after annealing at a temperature high enough, which is due to desorption of hydrogen from the surface.

The loss of chemisorbed hydrogen from diamond surfaces requires temperatures of $\sim 700^\circ\text{C}$ to occur with any significant rate[22], so the simple loss of surface hydrogen would not appear to account for the observations made here at temperature lower than 600°C in vacuum. However, the loss of hydrogen from diamond could occur at temperatures lower than 300°C in air due to oxidation[23].

The fact that the sheet carrier density remains in the range of 10^{12} - 10^{13} cm^{-2} following an annealing process below 250°C in air and 600°C in vacuum suggests that the fabrication of

devices which would operate up to this temperature using hydrogenation as a source of carriers appears viable.

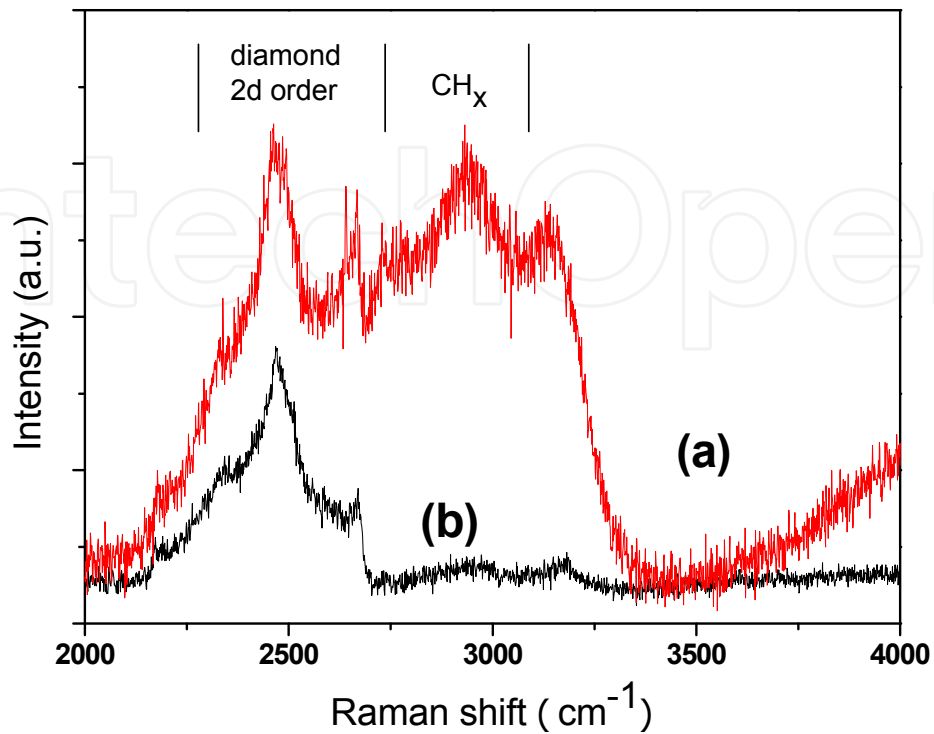


Fig. 11. Ultraviolet Raman scattering spectra for hydrogenated diamond nucleation surface sample (a) and annealed diamond surface sample (b)

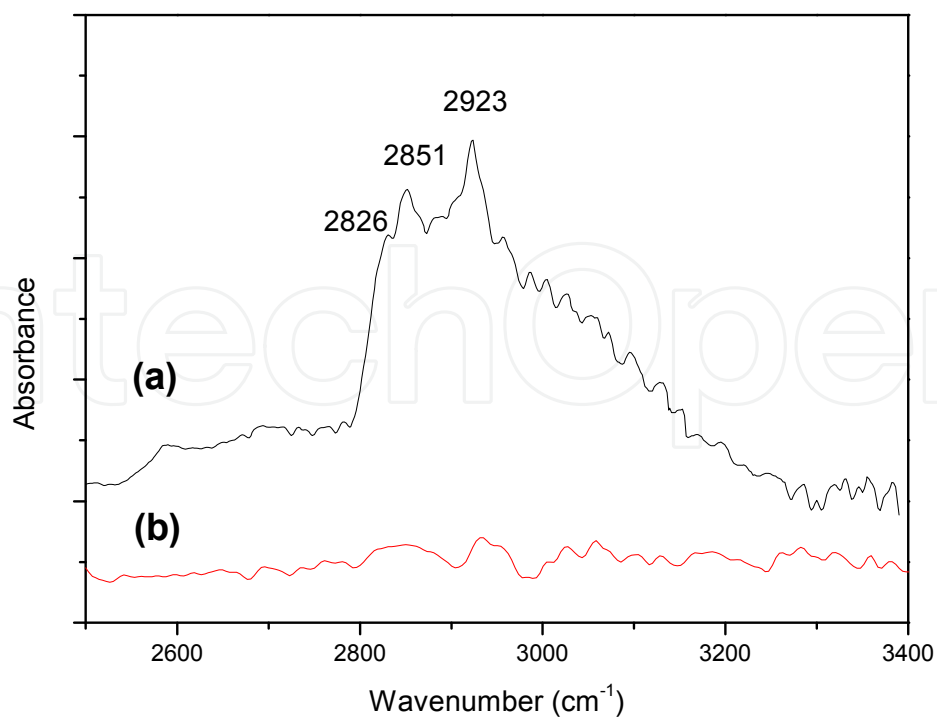


Fig. 12. Infrared spectra for hydrogenated diamond nucleation surface sample (a) and annealed diamond surface sample (b)

In order to take a further insight into surface conductivity of the nucleation surface of diamond films, the ultraviolet Raman scattering spectroscopy was used to characterize hydrogenated nucleation surface of diamond sample (a) and 500°C annealed (in air) diamond surface sample (b). The magnified profiles of ultraviolet Raman scattering spectra scanned in the 2000 -4000 cm^{-1} region were shown in Fig. 11. From the figure, sample (a) and sample (b) both had a strong peak at about 2468.49 cm^{-1} , representing the second order of the diamond peak, and a weaker peak at about 2669.52 cm^{-1} and at 3148.26 cm^{-1} , representing the second order of the D band and G band of graphine respectively. However, sample (a) had a stronger peak at 2930.93 cm^{-1} which indicates $\text{sp}^3 \text{CH}_x$ [24], in comparison with annealed nucleation surface of sample (b). It meant that, after annealed at a temperature of 500 °C in air, hydrogen desorbed from the nucleation surface of FSD films.

The internal reflection infrared spectrum obtained from sample (a) hydrogenated nucleation surface of diamond and sample (b) 500°C annealed (in air) diamond surface were shown in Fig. 6, from which the symmetric C-H stretching modes s at 2826 cm^{-1} , symmetric stretching mode of CH_2 at 2851 cm^{-1} and the antisymmetric stretching mode of CH_2 at 2923 cm^{-1} can be observed in films after hydrogen plasma treatment[23,25]. However, there was no obvious hydrocarbon adsorbates from the spectrum of Fig. 11(b) obtained after annealing at 500 °C in air, which indicated that the hydrogen desorbed from the surface of diamond film after annealing. All the above results confirmed that the diamond surface conductivity was related to the complexes of absorbed hydrogen atoms with carbon dangling bonds.

4. Fabrication and characterization of phototransistor based on diamond MESFETs

The FSD films were used to fabricate devices of MESFET. The fabrication of surface devices using the nucleation surface of the FSD films solved the problem of the surface roughness without the need of any kind of polishing. The smoothness of the nucleation surface allows a higher control of the electrodes. And the problem of the high resistivity can be easily overcome by a proper exposure of the surface to hydrogen plasma, as described above. FSD films using for device fabrication were prepared as described in paragraph 2. Then, FSD films were exposed to hydrogen plasma at 750°C for 30min using a MPCVD apparatus.

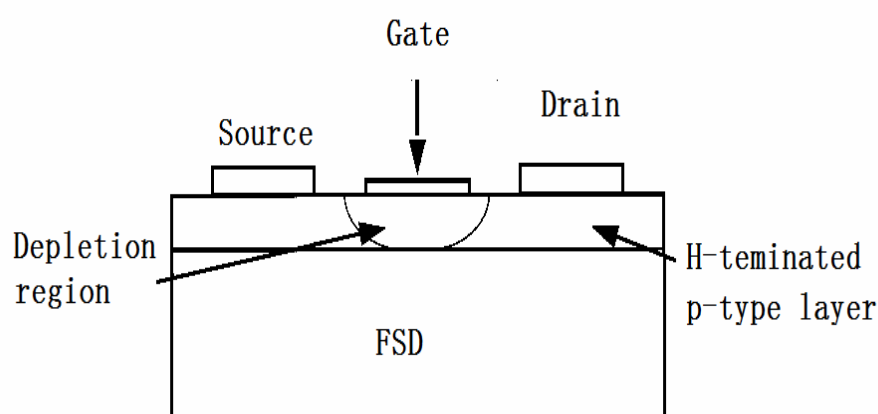


Fig. 13. A schematic the diamond MESFET device structure

Gold Ohmic contacts were evaporated as source (S), drain (D) and Aluminum contacts as gate (G) by standard lithographic procedures. The thickness of the drain/source and gate

contacts was 300nm and 200nm, respectively. The channel length and width were 10 μm and 5 μm , respectively. The distance between Al electrode and Au electrode is about 10 μm . A schematic picture of the device structure and optical micrograph of the device were shown in Fig. 12 and Fig.13, respectively. All devices were packaged and wire bonded prior to testing.

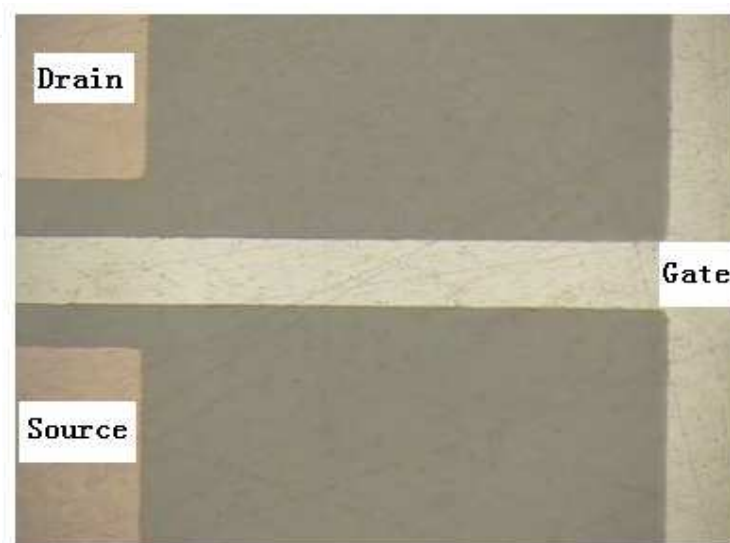


Fig. 14. Optical micrograph of the MESFET device

Current-Voltage (I-V) behaviour of the gold-gold electrodes and aluminum-gold electrodes on Hydrogen-terminated nucleation surface of FSD films were shown in Fig.14 (a) and Fig.14 (b). The I-V characteristics of adjacent Au contacts were near to linear, indicating Ohmic-like behavior, however Al-Au electrodes showed a strongly asymmetric I-V behavior, due to the presence of a Schottky barrier at the Al-diamond interface.

Figure 15 showed the Current-Voltage (I-V) behaviour of the source and drain electrodes without any applied gate voltage. The gold electrodes, evaporated directly on the Hydrogen-terminated nucleation surface of FSD films, behave as ohmic contacts. The small asymmetry in the characteristics is related probably with a slight heating of the electrode when the current starts to flow, increasing the resistivity of the material and producing an extra decrease of the current [26].

Hydrogen-terminated FSD film MESFET structures, with an Al gate and Au source and drain contacts, showed clear modulation of channel current as a gate bias was applied. The drain current as a function of drain-source voltage (V_{DS}) plotted for differing gate bias (V_{GS}) was shown in Fig.16. Field effect was seen for negative V_{GS} , revealing a p-channel. There was no current for $V_{GS} = 0$ V, and channel current considerably increased as V_{GS} was increased, indicating the device was an enhancement-mode MESFET. For all gate bias values, I_{DS} saturated for higher V_{DS} , indicating channel pinch-off.

Figure17 showed I_{DS} against V_{DS} with gate voltages of -0.1V which was illuminated with 200 nm light with varying intensity. The effect of the light is clearly to enhance the channel current level, with increasing optical powers giving higher saturated I_{DS} values. The results suggest that phototransistors based on hydrogenated diamond MESFETs may be ideally suited for UV switching applications. The devices are not "visible blind" in the way that photoconductive structures can be, but they do offer the potential of high switching speed allied to high sensitivity.

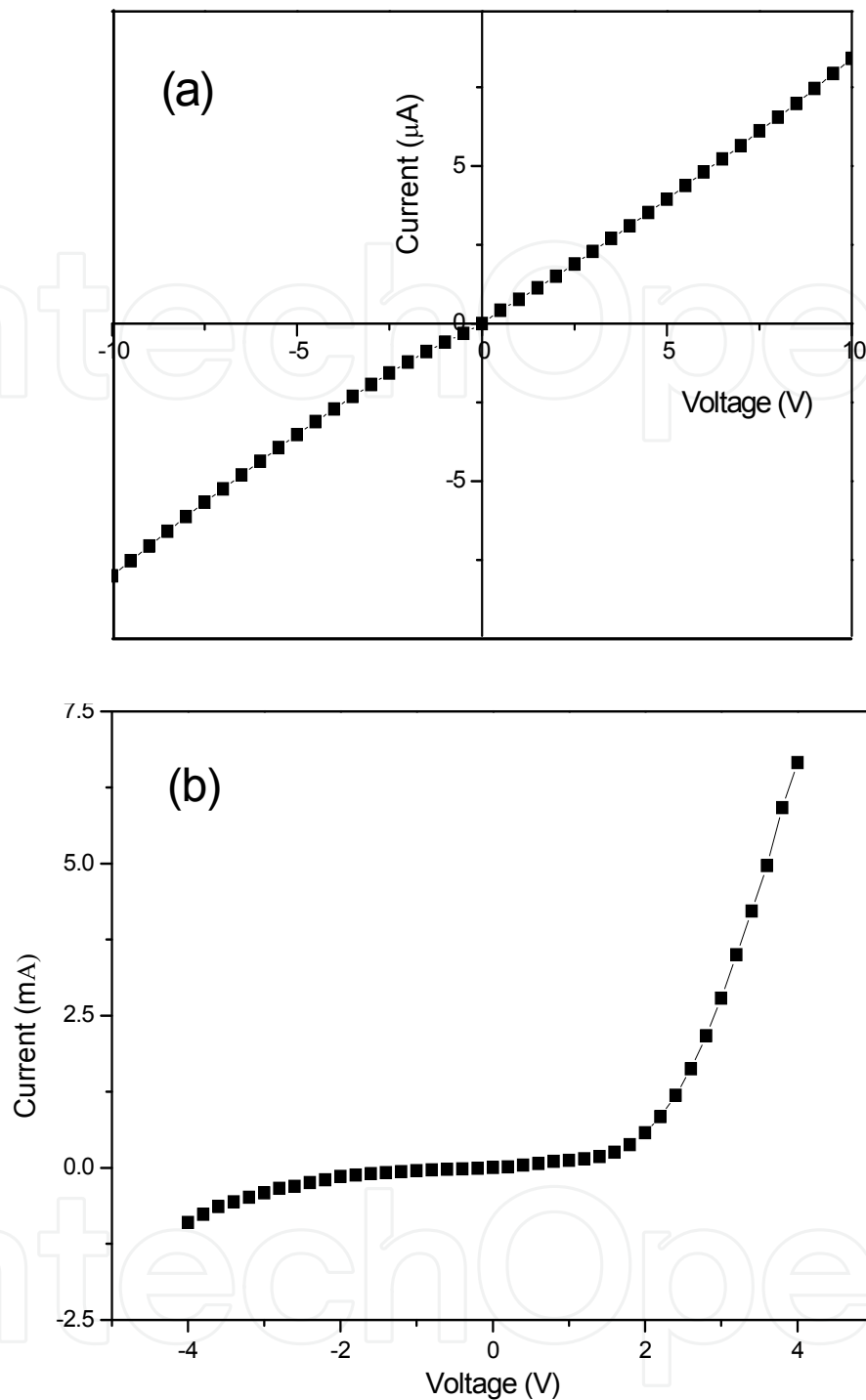


Fig. 15. Current-Voltage behaviour of the gold-gold electrodes (a) and aluminum-gold electrodes (b)

A PTI optical system and monochromator combination was used to investigate the response of the device across the spectral range 200–350 nm. Responsivity of diamond phototransistors as a function of illuminating wavelength with V_{DS} of -12V was shown in Fig.18. For the phototransistor, a pronounced increase in responsivity could be seen at around 230 nm, which corresponds to the band-gap energy of diamond. The response at the longer wavelengths (>300nm) was much smaller.

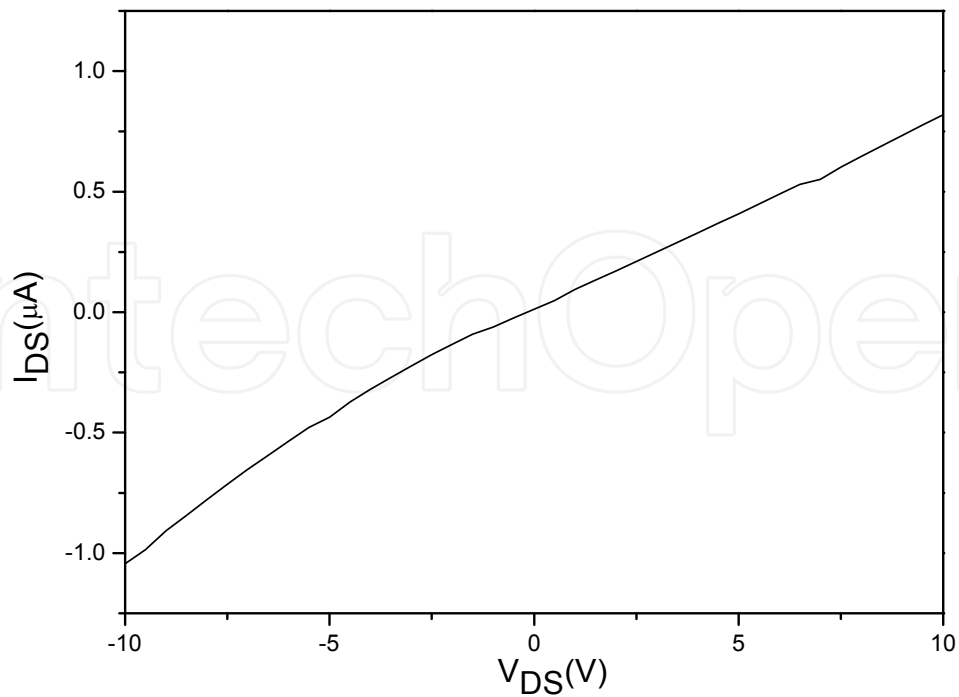


Fig. 16. Current-Voltage behaviour of the source and drain electrodes without any applied gate voltage

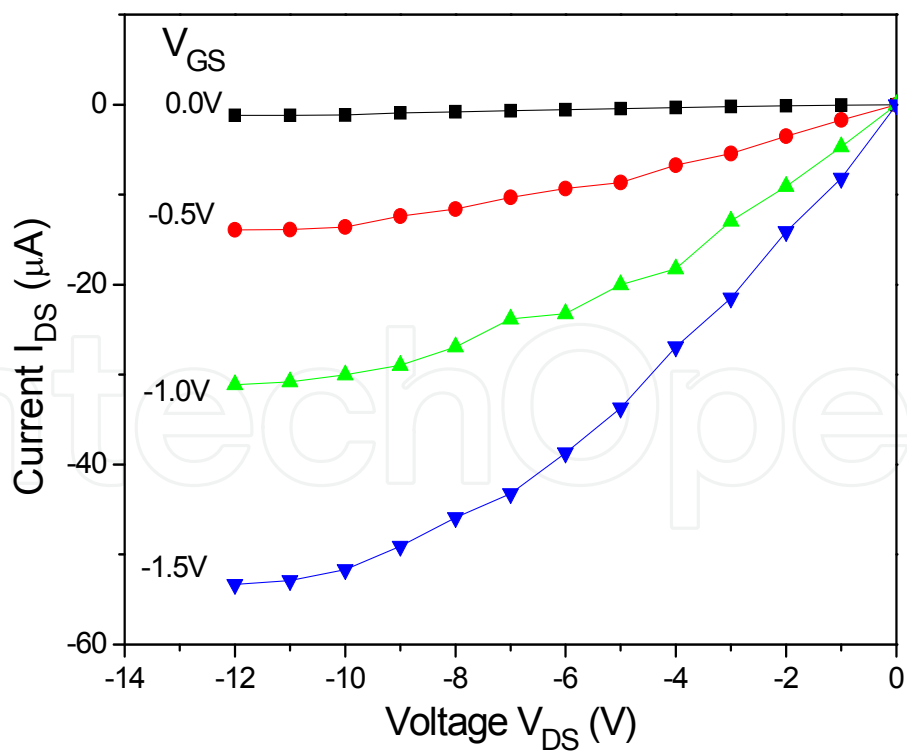


Fig. 17. Output characteristics of Hydrogen-terminated FSD film MESFET structures for negative bias. Drain-source voltage (V_{DS}) swept between 0 and -12 V; gate voltages (V_{GS}) swept between 0 and -1.5 V

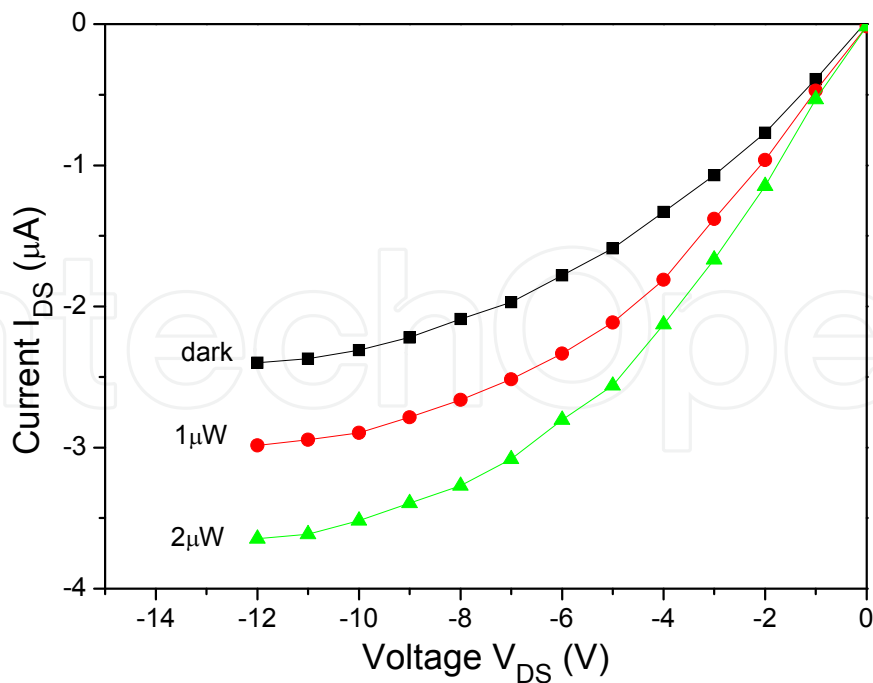


Fig. 18. Drain current against drain-source voltage for differing illumination power ($\lambda = 200$ nm) with gate voltages of -0.1 V

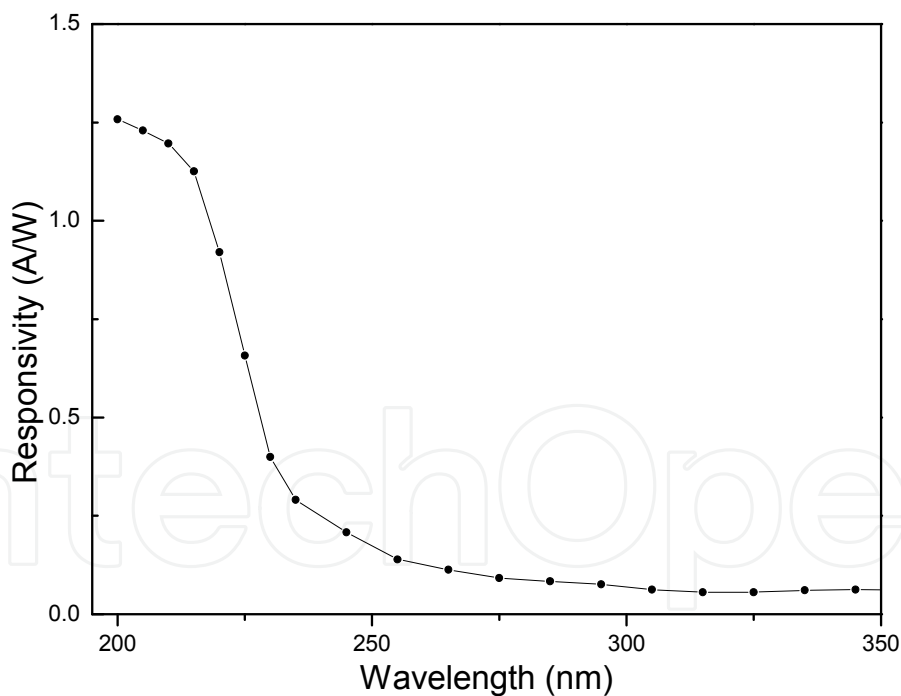


Fig. 19. Responsivity of diamond phototransistors as a function of illuminating wavelength with V_{DS} of -12 V

5. Conclusions

In this work, high quality freestanding diamond (FSD) films were grown by microwave plasma chemical vapor deposition (MPCVD) method. The effects of hydrogen plasma

treatment and annealing process on the p-type behavior of FSD films were investigated. The origin of this high-conductivity layer of FSD films was also discussed. The fabrication and properties of phototransistors based on hydrogenated diamond MESFETs were studied. The main conclusions of the work were as below:

1. The thickness of FSD films, the structure, and morphology of the FSD nucleation surface were analyzed by scanning electron microscopy (SEM), atomic force microscopy (AFM), and Raman spectroscopy. The results indicated that the nucleation sides of FSD films prepared by both methods were very smooth with a mean surface roughness of about 10 nm in a scanning area of $1.5 \times 1.5 \mu\text{m}^2$. The thickness of the film was about $110 \mu\text{m}$. The Raman results showed a high quality diamond of nucleation side of FSD diamond films with low content of non-diamond carbon. The post-treatment (wet chemical etch, annealing process) was helpful to improve the quality of FSD films.
2. The nucleation sides of FSD films prepared by MPCVD method were exposed to hydrogen plasma treatment. The effects of hydrogen plasma treatment and annealing process on the p-type behavior of FSD films were investigated. The origin of this high-conductivity layer of FSD films was also discussed by using ultraviolet (UV) Raman spectroscopy, Fourier-transform infrared spectroscopy (FTIR) and secondary ion mass spectrometry (SIMS). The nucleation side of FSD films with a p-type conductivity layer ($\sim 50 \text{nm}$ thick) could be obtained by hydrogen plasma treatment; The origin of this conductivity layer may be related to the complexes of absorbed hydrogen atoms with carbon dangling bonds; The sheet carrier concentration of the FSD film increased and sheet resistivity decreased with the time (5-30min) of plasma treatment; Surface conductivity of hydrogenated diamond surfaces disappeared gradually after annealing at temperature above 200°C in the air, or above 600°C in the vacuum.
3. The properties of metal contacts on hydrogenated p-type diamond surfaces were discussed. The results suggested that ohmic contacts could be realized between the p-type diamond and the Au electrodes. However, it's easy to form schottky contacts between Al electrodes and the p-type diamond. Preparation and properties of phototransistors based on hydrogen-terminated diamond film p-type channel metal-semiconductor field effect transistors (MESFETs) were reported. The results showed a typical characteristic of enhancement-mode MESFET and the phototransistor may be ideally suited for UV switching applications. The phototransistor showed a pronounced increase in responsivity at around 230 nm, which corresponds to the band-gap energy of diamond.

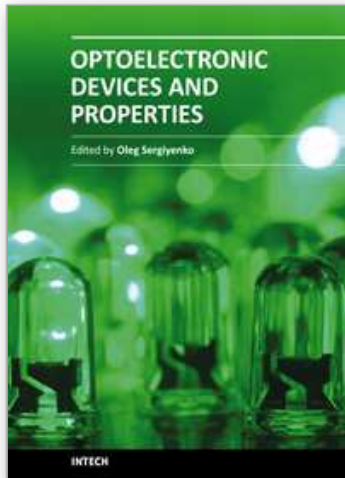
6. Acknowledgments

This work was supported by National Natural Science Foundation of China (60877017), Program for Changjiang Scholars and Innovative Research Team in University (No:IRT0739), Shanghai Leading Academic Disciplines (S30107) and Innovation Program of Shanghai Municipal Education Commission (08YZ04).

7. References

- H. L. Lu, Y. M. Zhang, Y. M. Zhang, et al. A comprehensive model of frequency dispersion in 4H-SiC MESFET [J]. *Solid-State Electronics*, 2009, 53: 285-291.
- Yasuhiro Ueda, Yasuhiko Nomura, Seiji Akita, et al. Characteristics of 4H-SiC Pt-gate metal-semiconductor field-effect transistor for use at high temperatures [J]. *Thin Solid Films*, 2008, 517: 1468-1470.

- Yuki Niiyama, Hiroshi Kambayashi, Shinya Ootomo, et al. 250 °C operation normally-off GaN MOSFETs [J]. *Solid-State Electronics*, 2007, 51:784-787.
- E. Tschumak, M. P. F. deGodoy, D. J. As, et al. Insulating substrates for cubic GaN-based HFETs [J]. *Microelectronics Journal*, 2009, 40: 367-369.
- M. Bavdaz, A. Peacock, A. Owens. Future space applications of compound semiconductor X-ray detectors [J]. *Nucl. Instr. and Meth. A*, 2001, 458: 123-131.
- M. Schieber, H. Hermon, A. Zuck, et al. Theoretical and experimental sensitivity to X-rays of single and polycrystalline HgI₂ compared with different single-crystal detectors [J]. *Nucl. Instr. and Meth. A*, 2001, 458: 41-46.
- E. Rossa, C. Bovet, D. Meier, et al. CdTe photoconductors for LHC luminosity monitoring [J]. *Nucl. Instr. and Meth. A*, 2002, 480: 488-493.
- I. M. Buckley-Golder, R. Bullough, M.R. Hayns, et al. Post-processing of diamond and diamond films: a review of some Harwell work [J]. *Diam. Relat. Mater.*, 1991, 1 (1) : 43-50.
- Yi Zhang, Linjun Wang, Qi Xiao, et al. The research on the surface structure and conductivity of free-standing diamond films for photo-transistor applications. *Proc. of SPIE*, 2009, 7381: 73811M-1--73811M -4.
- Qian Fang, Linjun Wang, Qingkai Zeng, et al. Preparation and photoelectric properties of a thin-film nanocrystalline diamond phototransistor, *Proc. of SPIE*, 2009, 7381: 73811N-1-73811N -4.
- K. Hayashi, S. Yamanaka, H. Okushi and K. Kajimura. *Appl. Phys. Lett.* , 1996,68:376-379.
- A. Aleksov, A. Denisenko, N. Kab, W. Ebert, E. Kohn, Diamond power FET concept. *Proceedings of the 2000 IEEE/ Cornell Conference on High Performance Devices*, Cornell, USA, 2000: 266.
- P. Gluche, A. Aleksov, A. Vescan, W. Ebert, M. Birk, E. Kohn, First diamond power FET structure. *Proceedings of the Fifty- Fifth Device Research Conference, Book of Abstracts*, Fort Collins, CO, USA, 1997: 42.
- M. Silveira, M. Becucci, E. Castellucci, et al. Non-diamond carbon phases in plasma-assisted deposition of crystalline diamond films: a Raman study [J]. *Diamond Relat Mater*, 1993, 2 (9): 1257-1262.
- Y. Bar-Yam and T. D. Moustakas. Defect-induced stabilization of diamond films [J]. *Nature*, 1989, 342: 786 - 787.
- J. Nan and I. Toshimichi. Electrical properties of surface conductive layers of homoepitaxial diamond films [J]. *JOURNAL OF APPLIED PHYSIC*, 1999, 85(12): 8267-8273.
- J. Nan, H. Akimitsu and I. Toshimichi. Nitrogen Doping Effects on Electrical Properties of Diamond Films [J]. *Jpn. J. Appl. Phys.*, 1998, 37: L1175-L1177.
- C. Su, J.-C. Lin. Thermal desorption of hydrogen from the diamond C(100) surface [J]. *Surface Science*, 1998, 406: 149-166.
- F. Maier, M. Riedel, B. Mantel, et al. Origin of Surface Conductivity in Diamond [J]. *PHYSICAL REVIEW LETTERS*, 2000, 85 (16): 3472-3475.
- D. Ballutaud, T. Kociniewski, J. Vigneron, et al. Hydrogen incorporation, bonding and stability in nanocrystalline diamond films [J]. *Diamond & Related Materials*, 2008, 17: 1127-1131.
- C. L. Cheng, C F. Chen, W. C. Shaio, et al. The CH stretching features on diamonds of different origins [J]. *Diamond & Related Materials*, 2005, 14: 1455 - 1462.
- J. C. Madaleno, L. Pereira, G. Lavareda, , et al. A MIS transistor using the nucleation surface of polycrystalline diamond [J]. *Diamond & Related Materials*, 2008,17 : 768 - 771.



Optoelectronic Devices and Properties

Edited by Prof. Oleg Sergiyenko

ISBN 978-953-307-204-3

Hard cover, 660 pages

Publisher InTech

Published online 19, April, 2011

Published in print edition April, 2011

Optoelectronic devices impact many areas of society, from simple household appliances and multimedia systems to communications, computing, spatial scanning, optical monitoring, 3D measurements and medical instruments. This is the most complete book about optoelectromechanic systems and semiconductor optoelectronic devices; it provides an accessible, well-organized overview of optoelectronic devices and properties that emphasizes basic principles.

How to reference

In order to correctly reference this scholarly work, feel free to copy and paste the following:

Linjun Wang, Jian Huang, Ke Tang, Jijun Zhang and Yiben Xia (2011). Thin-Film Diamond Phototransistors, Optoelectronic Devices and Properties, Prof. Oleg Sergiyenko (Ed.), ISBN: 978-953-307-204-3, InTech, Available from: <http://www.intechopen.com/books/optoelectronic-devices-and-properties/thin-film-diamond-phototransistors>

INTECH
open science | open minds

InTech Europe

University Campus STeP Ri
Slavka Krautzeka 83/A
51000 Rijeka, Croatia
Phone: +385 (51) 770 447
Fax: +385 (51) 686 166
www.intechopen.com

InTech China

Unit 405, Office Block, Hotel Equatorial Shanghai
No.65, Yan An Road (West), Shanghai, 200040, China
中国上海市延安西路65号上海国际贵都大饭店办公楼405单元
Phone: +86-21-62489820
Fax: +86-21-62489821

© 2011 The Author(s). Licensee IntechOpen. This chapter is distributed under the terms of the [Creative Commons Attribution-NonCommercial-ShareAlike-3.0 License](#), which permits use, distribution and reproduction for non-commercial purposes, provided the original is properly cited and derivative works building on this content are distributed under the same license.

IntechOpen

IntechOpen